Journal of Advanced Research 56 (2024) 157–165

Contents lists available at ScienceDirect

Journal of Advanced Research

journal homepage: www.elsevier.com/locate/jare

Original Article

A novel tree shrew model of lipopolysaccharide-induced acute respiratory distress syndrome

Jun He [a,1,*], Yue Zhao [a,1], Zhenli Fu [b,1], Li Chen [c,1], Kongzhen Hu [d], Xiaoyan Lin [a], Ning Wang [a], Weijian Huang [a], Qi Xu [a], Shuhua He [a], Ying He [b], Linliang Song [a], Mei xia Fang [a], Jie Zheng [e], Biying Chen [f], Qiuyan Cai [c], Jiangnan Fu [a], Jin Su [b,*]

[a] Institute of Laboratory Animal Science, Jinan University, Guangzhou, China
[b] State Key Laboratory of Respiratory Disease, National Clinical Research Center for Respiratory Disease, Guangzhou Institute of Respiratory Health, the First Affiliated Hospital of Guangzhou Medical University, Guangzhou, China
[c] Department of Respiratory and Critical Care Medicine, the First Affiliated Hospital of Jinan University, Guangzhou, China
[d] Nanfang PET Center, Department of Nuclear Medicine, Nanfang Hospital, Southern Medical University, Guangzhou, China
[e] Department of Food Science and Engineering, Jinan University, Guangzhou, China
[f] Radiology Department of the First Affiliated Hospital of Jinan University, Guangzhou, China

HIGHLIGHTS

- The LPS-induced tree shrews exhibited severe shortness of breath, resulting in hypoxemia.
- The induced group of animals exhibited 72 ~ 120 h endpoints, and none of them recover.
- Diffuse alveolar damage was observed in the lungs of the tree shrew, which is the histological hallmark for the acute phase of ARDS.
- 3D reconstruction of the lung CT images was used to accurately measure the extent and distribution of the whole lung injury in LPS-induced tree shrews.

GRAPHICAL ABSTRACT

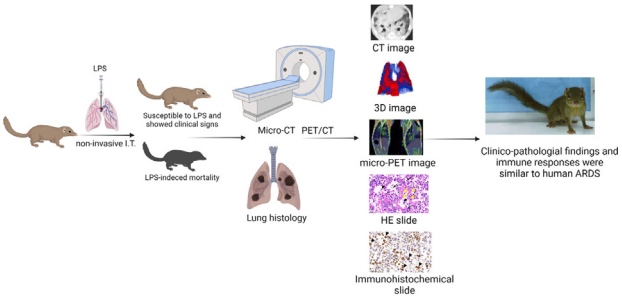

The workflow of one-hit LPS-induced ARDS tree shrew model. This figure was created by Biorender (https://app.biorender.com/).

ARTICLE INFO

Article history:
Received 7 May 2022
Revised 20 December 2022
Accepted 25 March 2023
Available online 8 April 2023

Keywords:
Tree shrew
Acute respiratory distress syndrome
Lipopolysaccharide
One-hit

ABSTRACT

Introduction: Acute respiratory distress syndrome (ARDS) is a leading cause of respiratory failure, with substantial attributable morbidity and mortality. The small animal models that are currently used for ARDS do not fully manifest all of the pathological hallmarks of human patients, which hampers both the studies of disease mechanism and drug development.
Objectives: To examine whether the phenotypic changes of primate-like tree shrews in response to a one-hit lipopolysaccharides (LPS) injury resemble human ARDS features.
Methods: LPS was administered to tree shrews through intratracheal instillation; then, the animals underwent CT or PET/CT imaging to examine the changes in the structure and function of the whole lung. The lung histology was analyzed by H&E staining and immunohistochemical staining of inflammatory cells.
Results: Results demonstrated that tree shrews exhibited an average survival time of 3–5 days after LPS insult, as well as an obvious symptom of dyspnea before death. The ratios of PaO_2 to FiO_2 (P/F ratio) were close to those of moderate ARDS in humans. CT imaging showed that the scope of the lung injury in tree

* Corresponding authors at: State Key Lab of Respiratory Diseases, National Clinical Research Center for Respiratory Disease, Guangzhou Institute of Respiratory Health, The First Affiliated Hospital, Guangzhou Medical University, Guangzhou, China (J. Su).
E-mail addresses: hejun@jnu.edu.cn (J. He), sujin@gird.cn (J. Su).
[1] These authors contributed equally to this work.

https://doi.org/10.1016/j.jare.2023.03.009

shrews after LPS treatment were extensive. PET/CT imaging with ^{18}F-FDG displayed an obvious inflammatory infiltration. Histological analysis detected the formation of a hyaline membrane, which is usually present in human ARDS.

Conclusion: This study established a lung injury model with a primate-like small animal model and confirmed that they have similar features to human ARDS, which might provide a valuable tool for translational research.

Introduction

Acute respiratory distress syndrome (ARDS) is a major clinical problem worldwide; it is caused by diffuse inflammation within hours to days after an injury to the pulmonary parenchyma, and it has few effective treatment options other than supportive mechanical ventilation [1]. Despite the great efforts made to understand the pathogenesis of ARDS and to improve the ability of intensive care therapy, the mortality rate of ARDS patients is still unacceptably high: in the range of 34.9–46.1%, depending on the severity of critically ill patients [2–4]. The New Berlin Definition for ARDS defined the disease as involving pathological changes in the lungs, including massive inflammation, acute severe hypoxemia, increased edema, diffuse alveolar hemorrhage, and the formation of hyaline membranes [5–7]. The pulmonary hyaline membrane—considered to be a blood derivative that is composed of a mixture of cellular debris, immunoglobulin, fibrin, and plasma protein—can impair gas exchange in clinical patients [6].

Although numerous pharmacological strategies have demonstrated effectiveness in animal studies, none of them have successfully been translated into practice [8,9]. A variety of animal species have been used for years in the study of ARDS, including both small and middle animals (mice, rats, and rabbits) as well as large animals (sheep, pigs, and dogs) [10–13]. Because mice and rats often die of shock upon LPS injury, the evaluation duration in these studies is usually no more than 24 h, and the researchers have to focus primarily on detecting inflammatory cytokines and pulmonary vascular permeability [14]. In addition, the hyaline membrane structure is rarely observed in small rodent species. The application of larger animal models requires both expertise manipulation and special feeding facilities, and their pathophysiology remains an ongoing controversy [10,15].

The tree shrew (*Tupaia belangeri chinensis*), which belongs to the family *Tupaiidae*, is a squirrel-like small mammal (about 120–150 g body weight) with many similar genomic and phenotypic features to primates [16]. Other advantages that make the tree shrew an ideal animal model include its easy breeding and rapid reproduction. As yet, this unique 'low-grade primate' has been widely used in multiple studies of human diseases, including myopia, depression, cancer, hepatitis, depression, drug addiction, bacterial infection, fibrosis, and thrombosis [17]. The immune responses in tree shrews were recently shown to resemble those in humans [18,19], and the usage of this species for immune-related research on viral infections is increasing, due to the animal's susceptibility to several human viral pathogens [20–22].

Animal models of ARDS can either simulate community-acquired pneumonia by intratracheal administration of bacterial LPS or reproduce aspiration pneumonia by injection of acid. Sepsis from pulmonary or non-pulmonary infections is still the most common etiology of ARDS [23]. The usage of LPS has been preferred in establishing animal models, particularly in small-animal studies [24,25].

In terms of the evaluation methodologies in ARDS animal studies, several pathological parameters have routinely been determined in both small and large animals, including inflammatory infiltration, vascular permeability, and alveolar hemorrhage [6]. In addition, Computed Tomography (CT) imaging of the lung, as well as continuous monitoring of the animal's respiratory syndrome and body weight, have also been performed in middle and large animal models [26,27].

In the current study, tree shrews were subjected to intratracheal instillation of high-dose LPS, and the ARDS-related manifestations were comprehensively investigated. The major findings here include the following: firstly, the one-hit LPS insult induced obvious ARDS, which occurred within 3–5 days after insult; secondly, both micro-CT and positron emission tomography (PET)/CT imaging techniques were used to provide dynamic data reporting on the structural and functional characteristics of the whole lungs; thirdly, the hyaline membrane that is absent in conventional small animals was prominently observed in tree shrews. Therefore, we provide compelling evidence that the tree shrew, as a 'small' but primate-like animal, can manifest many of the traits of human ARDS.

Materials and methods

Preparation of animals and ethical approval

The study protocol was approved by the Institutional Animal Care and Use Committee at Jinan University (No. IACUC-20191014-01). Experiments were performed on 2-years-old tree shrews, weighing 120 ~ 150 g (Animal Experimental Centre of Kunming Medical University, Kunming, China). Generally, put a tree shrew in each cage and was housed under controlled temperature (15 ~ 24 °C), lighting (12:12 h light–dark cycle), humidity (50 ~ 70%) conditions and provided with free access to food and sterile water. In addition, mealworms were supplied once a week.

LPS-induced lung injury model

In order to accurately determine the depth of the tracheal intubation, a tree shrew was firstly euthanized to detect the distance from the larynx to branch of the lobar bronchus. Tree shrews were intranasally with 180 ~ 200 mg/kg UltraPure LPS (*Escherichia coli* O111:B4, sc-221855B, Santa Cruz Biotechnology, USA). PBS group–Tree shrews were exposed to PBS and euthanized after 120 h; LPS group–Tree shrews were exposed to LPS and euthanized after observed clinical symptoms, and breathing difficulties (**Table s1**). The animals were premedicated by respiratory anesthesia of isoflurane within isoflurane (3.5%) and 0.8 free oxygen (Shenzhen Ryward Life Technology Co., Ltd., Shenzhen, China). After loss of consciousness, endotracheal intubation of tree shrews with modified child laryngoscope (simeite 2012–58, Jiangsu, China, **Figure s2**) and indwelling needle (16GA × 5.25IN, Becton Dickinson Medical Devices Co., Ltd, Suzhou, China, **Figure s3**) to tracheal LPS. Lung samples of each tree shrew was collected as shown in **Figure 1**, and lung lobe marked NO.7 were fixed in 4% buffered paraformaldehyde solution. An arterial blood gas sample catheter was placed in the abdominal aorta and blood gas analysis was

performed (SIEMENS Rapidpoint500, SIEMENS healthineers, Germany).

Micro-Computed tomography

Tree shrews were transferred to the microscopic computed tomography (PINGSENG Healthcare Inc., SNC-100, Jiangsu, China). The scanning was performed during end inspiratory hold (70 kV, 0.55 mA, 44*44*88 μm pixel size, 0.088 mm slice thickness). After being anesthetized with isoflurane, NO.1 tree shrew underwent lung imaging with high resolution micro-CT on days 0, 3 and 5 respectively. Transmit CT scan images to 3D Slicer software for analysis (https://www.slicer.org), such as segmentation, 3D reconstruction, and volumetric analysis. In order to accurately characterize global changes in the lung during LPS lesion progression, a manual segmentation is needed to correctly identify lung areas that cannot be clearly detected due to lack of aeration, jagged or severely damaged parenchyma and lack of clear boundaries. Briefly, the segmentation using region growth algorithm is semi-automatic. The lack of aeration regions was determined by manually drawing the outer boundary and the severely damaged lung parenchyma inside. Based on the CT attenuation densities, different aerated lung regions were divided into 4 categories: aerate area, −1000 to − 121 HU; non-aerated, −120 to 121 HU [28]. The airway and vessels were carefully eliminated by manually segmentation.

CT score

Both lungs were divided into the upper zone, middle zone, and lower zone. A respiratory physician and two researchers scored manually based on CT images. The degree of involvement of each lung zone was scored according to the following criteria: score 0 (no involvement), score 1 (< 25% involvement), score 2 (25% to < 50% involvement), score 3 (50% to < 75% involvement), and score 4 (> 75% involvement) [29].

Micro-PET/CT imaging

Dynamic micro-PET imaging studies were conducted in tree shrews using the InveonMicro PET/CT scanner (SIEMENS, Erlangen, Germany). After being anesthetized with isoflurane, tree shrews were injected intravenously within 14.8 ~ 18.5 MBq of ^{18}F-FDG into the animal through the tail vein and placed on a heating pad to maintain body temperature during the process. The animal's breathing and any other signs of pain were visually monitored throughout the entire imaging period. 10 min static PET images were acquired at 60 min post injection, and then the imaging started with a low-dose CT scan, shortly followed by a PET scan. The CT scan was used for attenuation correction and localization of lesion. The images were reconstructed by two-dimensional ordered-subsets expectation maximum (OSEM). For data analysis, the regions of interest (ROIs) were manually drawn over the inflammatory site and lung on decay-corrected whole-body coronal images using Inevon Research Workplace 4.1 software. The radioactivity concentration (accumulation) in the inflammatory site or lung was obtained from the averagen pixel values within the multiple ROI volume.

SUV-bw = Tissue concentration (Bq/g)/[injected dose (Bq)/body weight (g)].

Lung water content

At the end of experiment, the right upper lung of each tree shrew was harvested and weighed, as the wet weight; and then dried to a constant weight at −80 °C for 72 h, as the dry weight. The lungs were then wet-dry-ratios (W/D) were calculated.

Histopathological analysis and scoring

The left lower lungs of every tree shrew were embedded in paraffin, cut into 4 μm-thick slices and stained with hematoxylin and eosin (H&E). 10 fields were randomly selected on each slide to score the total lung injury as previously described [30]. Digital slide images were scanned using Pannoramic SCAN (3D Histech, Hungary) and pathological changes including necrosis, atelectasis, edema, hemorrhage, alveolar and interstitial inflammation, and hyaline membrane formation were observed and scored on scale of 0–4. The lung injury score referenced by Smith score was calculated as the sum of all individual injury scores [31]. The percentage of pulmonary alveolar area (PAA) and mean alveolar number (MAN) were calculated by morphological analysis. All the image calculation and analysis were performed by case viewer 2.4 (3D Histech, Hungary) and Image Pro Plus software 6.0 (Media Cybernetics, Silver Spring, USA).

Immunofluorescence and immunohistochemical analysis

Tissue sections for immunofluorescence were labeled with antibody F4/80 (Servicebio, GB11027, Wuhan Servicebio Trchnology Co., Ltd, China). Tissue sections were immunostained using anti–CD68 antibodies (Servicebio, GB11067, Wuhan Servicebio Trchnology Co., Ltd, China). Macrophages were immunostained and counted in randomly 10 high-power fields (HPF) and quantified with positive area density by using the Image Pro Plus software 6.0 (Media Cybernetics, Silver Spring, USA).

Statistical analysis

The results are expressed as means ± SD. The two groups' comparisons were made, using *t* test. Data were analyzed with GraphPad Prism software, version 8.0 (GraphPad Software Inc., La Jolla, CA, USA). A p value < 0.05 was considered statistically significant.

Results

The functional changes of tree shrew lungs in response to LPS insult

In order to dynamically characterize both the functional and the structural alterations in tree shrew lungs upon LPS treatment, 6 tree shrews received endotracheal instillation of LPS and then were subjected to both CT and PET/CT imaging at the indicated time points; once obvious dyspnea occurred, they were euthanized (**Figure 1a**). The symptoms of respiratory failure in all six animals were observed to occur between day 3 and day 5 (**Figure 1b**). During the evolution of the LPS-induced lung injury, all LPS-induced tree shrews exhibited obvious behavioral abnormalities starting on day 3, including less activity, piloerection, and tachypnea.

The P/F ratio is widely used to evaluate the severity of ARDS, as suggested by the 2012 New Berlin Definition of ARDS [32]. According to these guidelines, a P/F ratio of < 100 is severe ARDS, 100 to < 200 is moderate ARDS and 200 to < 300 is mild ARDS [33]. In this study, the P/F ratios of only three animals were documented at either day 3 or day 4; the rest of the tree shrews were close to death after deep anesthesia when this assay was conducted. Unlike the PBS-treated animals, which had an average P/F ratio of 300 mmHg, LPS-treated counterparts showed values of only 160–200 mmHg, with a severity close to moderate ARDS in humans (**Figure 1c**, **Table s1**). In addition, since the wet-to-dry (W/D) ratio is another important indicator of the integrity of pulmonary

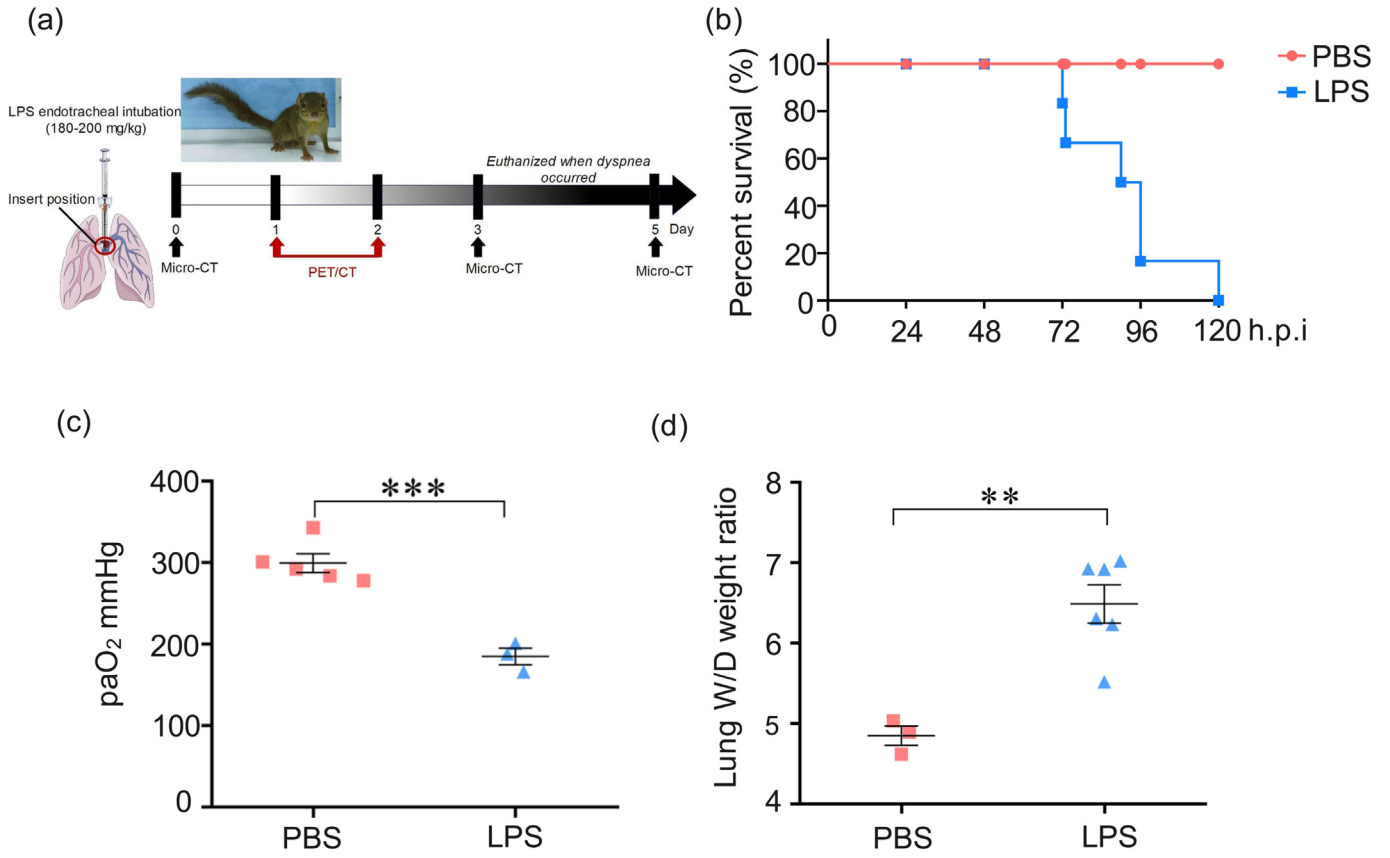

Figure 1. Acute lung injury following LPS-induced in tree shrews. (a) Workflow of induction of tree shrew by LPS intratracheally instilled. (b) The percent survival of PBS and LPS-induced tree shrews. (c) Arterial oxygenation (P/F) was evaluated following obvious symptoms of dyspnea. (d) Changes in alveolar-capillary barrier are measured by the wet-to-dry ratio (W/D). n = 3 ~ 6. $^{**}p < 0.01$, $^{***}p < 0.001$ vs PBS.

alveolar-capillary barrier function [34,35], this parameter was calculated for one lung lobe from all six animals after their euthanasia (**Online Supplementary Materials and method**). As shown in **Figure 1d**, the average lung W/D ratio in LPS-treated tree shrews was dramatically much higher than that in the PBS group. These results collectively demonstrated that a high dose of LPS was able to trigger a moderate-intensity ARDS response in tree shrews.

LPS challenge aggravates lung injury, as evaluated by micro-CT

As CT imaging can render the complete pictures of not only lung structure but also pulmonary aeration function [36,37], this non-invasive technique was applied to LPS-treated tree shrews at 3 or 5 days after injury. The CT images from the one animal that survived up to 5 days demonstrated that the consolidated areas (−120 to +121 HU) and aerate areas (−1000 to −121 HU) of the tree shrew lungs [28,38] were gradually enlarged before the advent of respiratory failure (**Figure 2a**), indicating the irreversible nature of LPS-induced lung injury in this species (**Figure s1**).

Because most LPS-insulted tree shrews started to show symptoms of respiratory failure at 3 ~ 5 days after treatment, the total volume of non-aerated regions in all six animal lungs was calculated at the time point of day 3 (**Table s2**). As demonstrated in the three-dimensional (3D) image (**Figure 2b**), LPS insult caused bilateral patchy infiltrates, which were particularly prominent at the basal parts of the lung, interlobar fissures, and lower lobes—a distribution pattern similar to that in clinical ARDS patients [38,39]. The ratios of non-aeration to total lung volume, observed in the CT images of all six animals on day 3, ranged from 20 to 70%, with an average value of 37% (**Figure 2c**).

Meanwhile, we used the traditional method (i.e., the lung score method part) to assess the lung injury in the LPS-induced tree shrews. As shown in **Figure 2d**, the overall CT score in the LPS-treated group at day 3 (range 14.0 ~ 23.9) was significantly higher than that in the PBS-treated group (range 0 ~ 5.3), which is consistent with the manifestation of the main features of an experimental ARDS model under the Berlin Definition (**Table s3**) [33]. Collectively, the distributed region of lung injury in the LPS-induced tree shrew model, as evaluated by micro-CT, triggered typical diffuse alveolar damage, which is consistent with ARDS patients.

Pulmonary inflammation, evaluated by ^{18}F-FDG PET

Since PET scan tracking of ^{18}F-fluorodeoxyglucose (^{18}F-FDG) uptake has been proven to reflect the neutrophil accumulation and activation in experimental ALI [40–42], this imaging technique was applied in our LPS-challenged tree shrew model. The representative coronal and sagittal images at 1 h after caudal vein injection of ^{18}F-FDG are shown in **Figure 3a**. The radioactivity signal was clearly visualized in the lung parenchyma in the LPS-treated group at 1 and 2 days, while no obvious signal was observed in the lung parenchyma in the PBS-treated group. Furthermore, micro-PET quantitative analysis showed that the ^{18}F-FDG standardized uptake value (SUV) mean of the pulmonary lung in the LPS-treated group was notably higher than that in the PBS-treated group (1.07 ± 0.10 vs. 0.23 ± 0.02 at day 1, 1.10 ± 0.08 vs. 0.27 ± 0.07 at day 2, $p < 0.001$; **Figure 3b**). These results indicate that the inflammation response of LPS-induced ARDS lungs in tree shrews occurred rapidly and persisted at a high level.

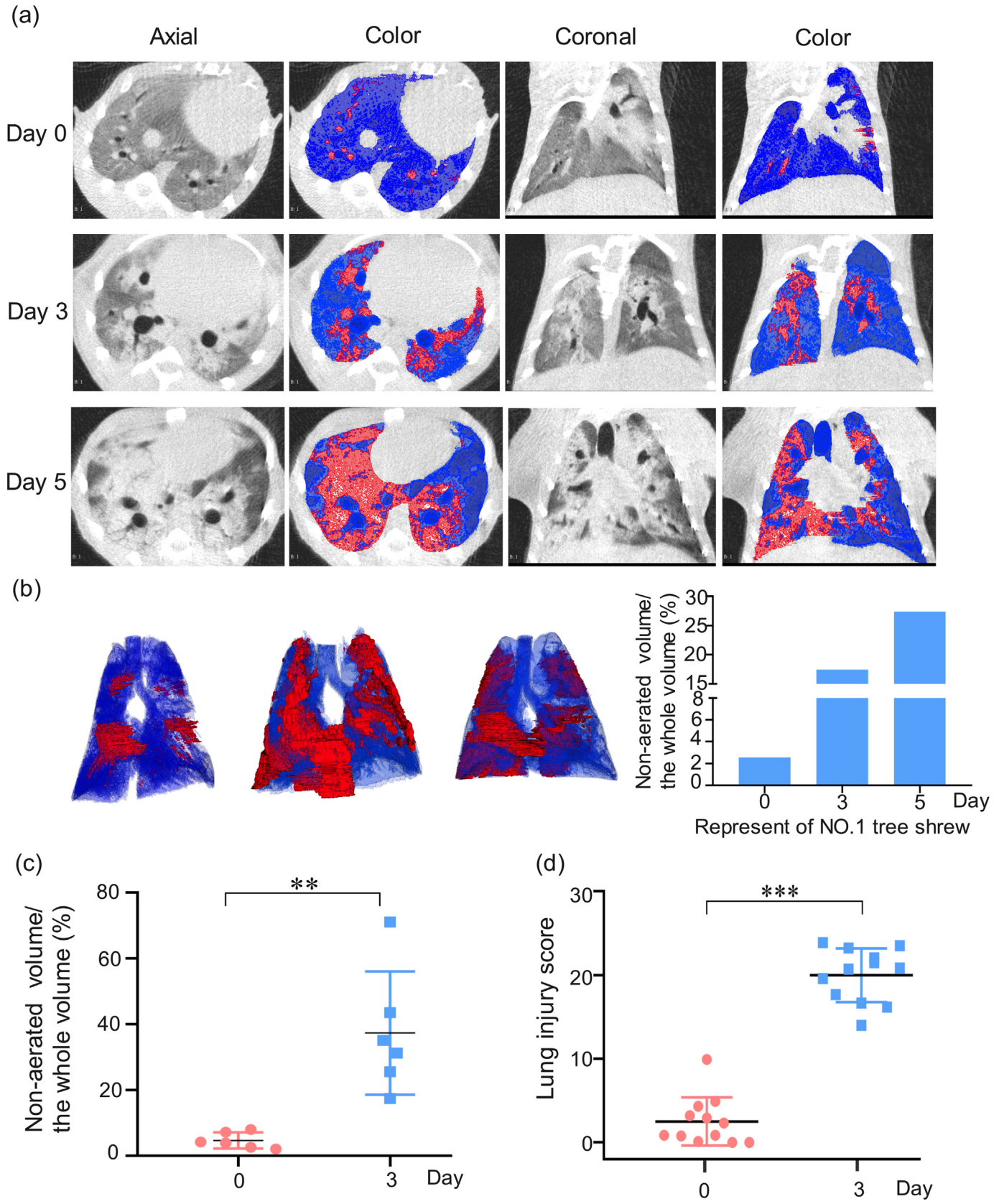

Figure 2. Micro-CT imaging of LPS-induced lung. (a) Representative micro-CT imaging of lung and colormap of NO.1 LPS-induced tree shrews at 0, 3, 5 days: transverse, coronal and color maps of transverse and coronal respectively. 3D renderings of LPS-infected tree shrew at day 0, 3, 5 with the aerated region ([−1000, −121] HU) in the blue and non-aerated region ([−120, +121] HU) in red. (b) Representative calculation of lung CT non-aerated volume of NO.1 tree shrew. (c) Quantitative CT volumetric evaluation of lung aeration. (d) Scoring the lung injury through the traditional analysis. n = 6, Data are expressed as mean ± SD, $^{**}p < 0.01$, $^{***}p < 0.001$.

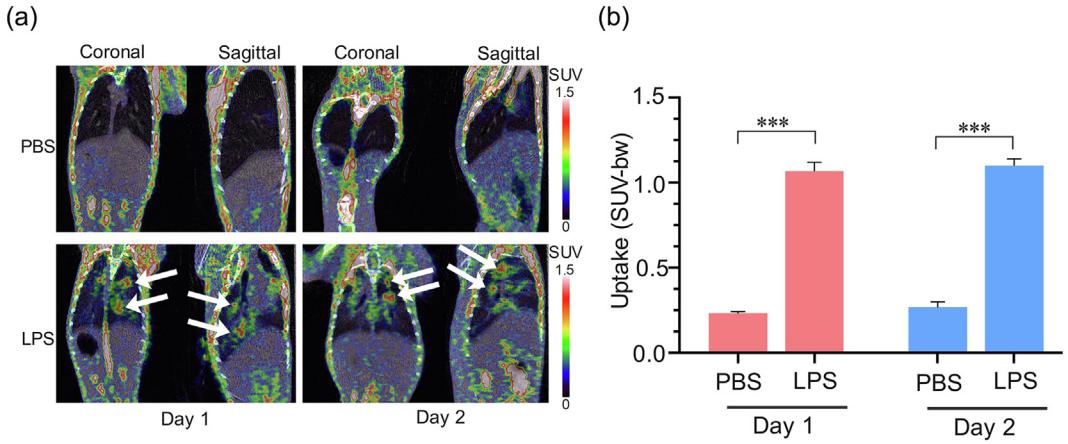

Figure 3. ^{18}F-FDG uptake on retention in the lung at the peak of immune response. Decay-corrected whole-body coronal and sagittal micro-PET images of LPS-treated. (a) and PBS-treated tree shrews a static scan at 1-h time point after injection of ^{18}F-FDG. The white arrows indicated the inflammatory site. (b) Comparing the uptake of ^{18}F-FDG in the lung of LPS-treated and PBS-treated (n = 3 ~ 5). Data are represented as mean ± SD. ***$p < 0.001$.

Lung histology

To further detect whether the pathological damage to the lungs of LPS-treated tree shrews is consistent with the pathological characteristics of human ARDS, we evaluated the histopathological changes through H&E staining. As shown in **Figure 4a** and **b**, the gross finding represented bilateral diffuse discoloration and focal consolation of the lung in the LPS group, which indicated obvious lung tissue injury in the tree shrews. The pathology results also revealed an array of increased cell counts, including neutrophils, macrophages, lymphocytes, which participate in inflammation. Compared to the normal pulmonary histological structures (**Figure 4c1 and c2**), the thickened alveolar septum (**Figure 4c4**), hemorrhage (**Figure 4c5**), edema, the proteinaceous debris filling the alveolar spaces and airspaces (**Figure 4c6**), the massive neutrophils (black arrowhead) accumulation, and infiltration were observed in the lungs of LPS-treated tree shrews, which was consistent with typical histopathological characteristics of human ARDS. Interestingly, the hyaline membrane (**Figure 4c4**, yellow arrow) was only observed in one lung of the experimental tree shrews, which makes it more similar to human ARDS than other small rodent models. Based on these histopathological changes, we combined lung injury score, MAN, and PAA analysis to semi-quantify the degree of lung injury. As shown in **Figure 4d**, **e**, and **f**, the degree of lung injury in LPS-treated tree shrews was dramatically more severe than that in the PBS-treated group.

Another typical pathological characteristic of human ARDS is potently increased alveolar macrophages, which is one of the main inflammatory cells involved in the pathogenesis of ARDS in humans and other animal models [43]. The alveolar macrophages—either immunohistochemically stained (brown particles) or immunofluorescence stained (green particles)—were abundantly greater in the LPS-treated group than in the PBS-treated group (**Figure 5a** and **b**). Further semi-analysis demonstrated that the number of macrophages and the positive area density in lungs of LPS-treated tree shrews were both significantly greater (**Figure 5c** and **d**). Collectively, the lung injury in the ARDS tree shrews exhibited bilateral diffuse discoloration, massive neutrophils accumulation, severe alveolar septum thickening, and hemorrhage: these fulfill the main criteria of the histological pattern of the diffuse alveolar damage in ARDS [14]. These results strongly suggest that the typical pathological changes of lung injury in LPS-treated tree shrews tends to be a serious pathological injury, which is consistent with the pathological injury in the New Berlin Definition of human ARDS.

Discussion

Our present findings showed that tree shrew models of ARDS triggered by a one-hit intratracheal instillation of LPS reproduced many of the characteristics of the acute phase of ARDS in human patients, such as prolonged endpoints, obvious symptoms of dyspnea, intensive inflammatory infiltration, and the formation of a hyaline membrane in the lung (**Figure 6**).

Unlike mouse and rat models of ARDS, which often die of shock after no more than 24 h of lung injury, the survival endpoints of all tree shrews used here ranged between 72 and 120 h. The long-lasting duration and non-resolution nature observed in tree shrew models is a typical feature seen in human ARDS patients [6], although it is in contrast with the self-resolved nature of ARDS in middle and large animal models (such as rabbits and sheep) [44]. In addition to the manifestation of survival, the P/F ratios of tree shrew models also matched the level of moderate ARDS patients, as established by the New Berlin Definition. Hence, from the aspects of survival duration and blood oxygen saturation in response to lung injury, tree shrews appear to be very similar to humans.

Using 3D quantitative assessments of lung CT imaging data, we found that the injured lesions in tree shrew lungs were predominantly located in the basal parts. Interestingly, these regions were also reported to be damaged in patients whose ARDS was caused by SARS-CoV-2 infection [39]. In contrast to traditional CT methods used in previous ARDS studies, which mostly demonstrate the lung images of one specific transverse section, here we not only provided the non-aeration regions across the whole lung but also calculated their total volumes through a recently developed algorithm [45]. Non-invasive quantitative assessment of the scope of lung injury might be particularly useful for future studies of both disease progression and drug therapy effects in ARDS.

It is well known that a higher W/D index and a massive infiltration of inflammatory cells are primary hallmarks of both ARDS patients and classical animal models [46]. These histological features were also observed as occurring in tree shrew lungs. In addition to pulmonary edema, hyaline membrane formation represents another important pathological change in ARDS patients; notably, the structure of a typical hyaline membrane was shown to be present in the lung of one injured tree shrew, even though it is rarely observed in small animal models [47]. This observation provides more evidence supporting the proximity between tree shrews and humans in ARDS response.

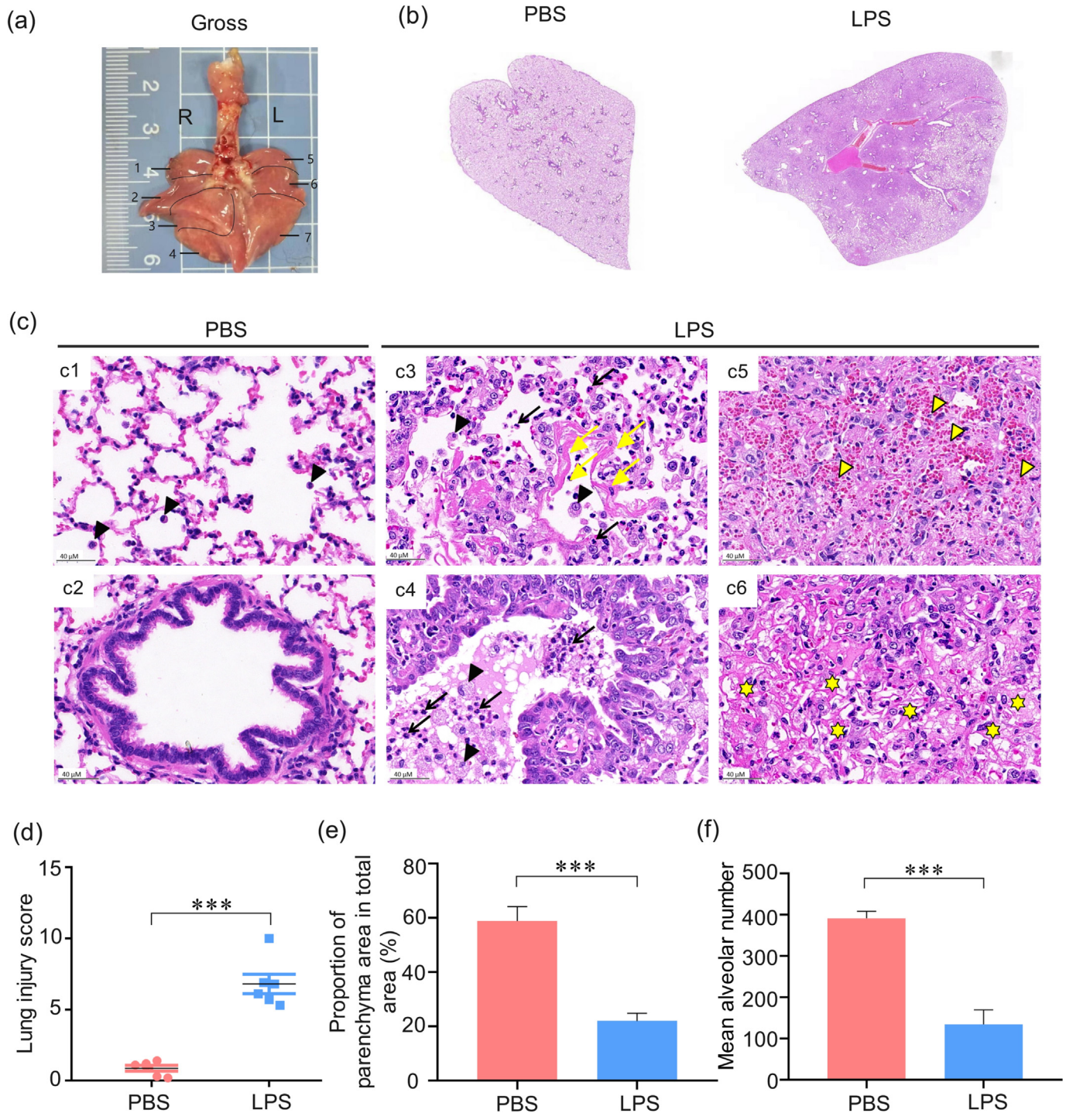

Figure 4. Histopathologic evaluation of lung injury from tree shrews after intratracheal instillation of LPS. (a) Gross finding of lungs from tree shrew represented obvious lobe discoloration. 3 lobes on the left side (L) and 4 lobes on the right side (R) of the whole lung of the tree shrew. (b) The whole lung pathological section of marked NO.7 lobe of the lung. (c) Representative images of pulmonary histopathology. The lung injury score (d), percentage of the pulmonary alveolar area (e), and mean alveolar number (f) of the LPS-induced tree shrew group. Black arrow: neutrophil, black arrowhead: macrophage, yellow arrowhead: erythrocyte, yellow arrow: hyaline membrane, yellow asterisk: exudate protein debris. ***$p < 0.001$ vs. PBS group (n = 6).

Although this study is the first to reveal that LPS-induced tree shrew lung injury manifests several of the same characteristics of human ARDS patients, a number of questions still need to be addressed in future studies. First, can longer survival of tree shrew ARDS models be established by lower dose of LPS? Second, can other types of conventional stimuli for ARDS (such as mechanical ventilation, smoke, and oleic acid) similarly induce human-like phenotypes of ARDS? Third, what kind of inducers or situations could exaggerate the formation of a hyaline membrane in tree shrew lungs? Finally, it is necessary to utilize well-validated antibodies against specific biomarkers of tree shrews in order to investigate the exact types of cells involved in the disease progression of ARDS [46].

To summarize, the data from this investigation suggest that tree shrews might represent the smallest species that can induce similar ARDS phenotypes to those found in humans, and thus these ani-

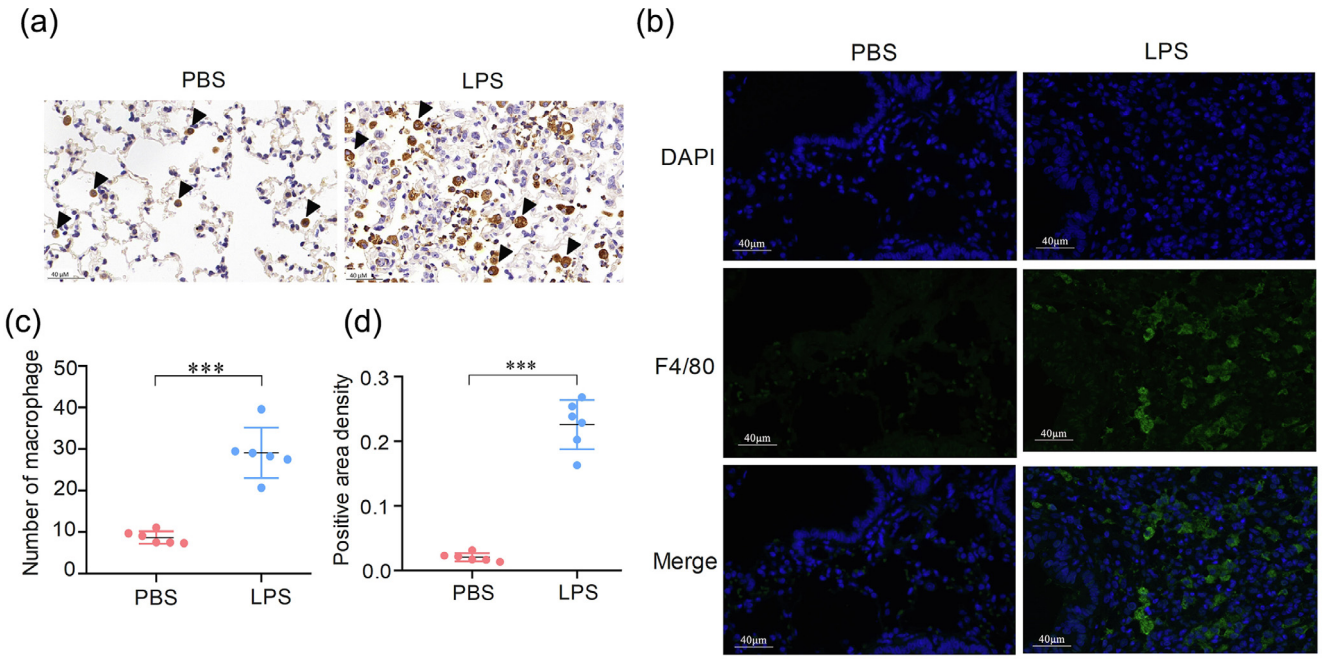

Figure 5. Counts for macrophages (green) increased in the ARDS group of tree shrews. (a) Slides stained immunohistochemically with CD68. Representative images of lungs from the PBS-treated and LPS groups of tree shrews. (b) Slides stained with F4/80 (green) antibodies. (c) The numbers of macrophages of HPF. (d) and Semi-analysis of positive area density revealed a significant difference between LPS and PBS-treated groups of tree shrews. ***$p < 0.001$ vs. PBS-treated group (n = 6).

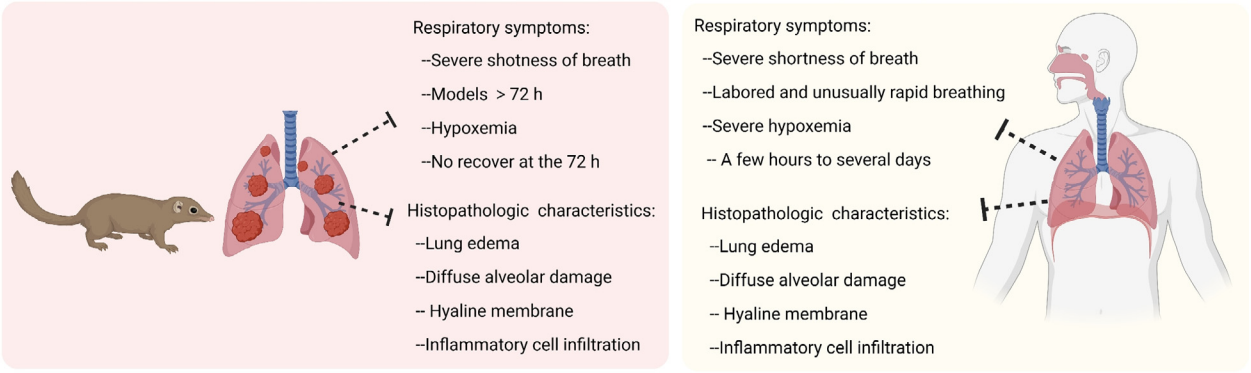

Figure 6. Several advantages of one-hit LPS-induced ARDS tree shrew models compared to human ARDS. The pictures showed the signs and symptoms of tree shrew model and human. This figure was created by Biorender (https://app.biorender.com/).

mals could serve as a feasible model for preclinical evaluations of ARDS drugs.

Declaration of Competing Interest

The authors declare that they have no known competing financial interests or personal relationships that could have appeared to influence the work reported in this paper.

Acknowledgements

This work was financially supported by the Basic and Applied Basic Research Fund of Guangdong Province (Grant Nos. 2021A1515010822 and 2019A1515011994), the National Natural Science Foundation of China (Grant No. 32273036) and the Fundamental Research Funds for the Central Universities (Grant No. 21620107).

Appendix A. Supplementary data

Supplementary data to this article can be found online at https://doi.org/10.1016/j.jare.2023.03.009.

References

[1] Matthay MA. ECMO in severe acute respiratory distress syndrome. Lancet Respir Med 2019;7(2):106–8.
[2] Lee SA, Lee SH, Kim JY, Lee WS. Effects of glycyrrhizin on lipopolysaccharide-induced acute lung injury in a mouse model. J Thorac Dis 2019;11(4):1287–302.
[3] Yu Y, Xu D, Fu S, Zhang J, Yang X, Xu L, et al. Patients with COVID-19 in 19 ICUs in Wuhan, China: a cross-sectional study. Crit Care 2020;24(1):219.
[4] Santos RS, Silva PL, Rocco JR, Pelosi P, Rocco PR. A mortality score for acute respiratory distress syndrome: predicting the future without a crystal ball. J Thorac Dis 2016;8(8):1872–6.
[5] Tang WH, Wang Z, Fan Y, Levison B, Hazen JE, Donahue LM, et al. Prognostic value of elevated levels of intestinal microbe-generated metabolite trimethylamine-N-oxide in patients with heart failure: refining the gut hypothesis. J Am Coll Cardiol 2014;64(18):1908–14.
[6] Matthay MA, Zemans RL, Zimmerman GA, Arabi YM, Beitler JR, Mercat A, et al. Acute respiratory distress syndrome. Nat Rev Dis Primers 2019;5(1):18.

[7] Zinter MS, Spicer AC, Liu KD, Orwoll BE, Alkhouli MF, Brakeman PR, et al. Positive cumulative fluid balance is associated with mortality in pediatric acute respiratory distress syndrome in the setting of acute kidney injury. Pediatr Crit Care Med 2019;20(4):323–31.
[8] Peck TJ, Hibbert KA. Recent advances in the understanding and management of ARDS. F1000Res 2019;8.
[9] Chimenti L, Morales-Quinteros L, Puig F, Camprubi-Rimblas M, Guillamat-Prats R, Gomez MN, et al. Comparison of direct and indirect models of early induced acute lung injury. Intensive Care Med Exp 2020;8(Suppl 1):62.
[10] Wang HM, Bodenstein M, Markstaller K. Overview of the pathology of three widely used animal models of acute lung injury. Eur Surg Res 2008;40 (4):305–16.
[11] Ballard-Croft C, Wang D, Sumpter LR, Zhou X, Zwischenberger JB. Large-animal models of acute respiratory distress syndrome. Ann Thorac Surg 2012;93 (4):1331–9.
[12] Sekiya Y, Shimada K, Takahashi H, Kuga C, Komachi S, Miwa K, et al. Evaluation of a simultaneous adsorption device for cytokines and platelet-neutrophil complexes in vitro and in a rabbit acute lung injury model. Intensive Care Med Exp 2021;9(1):49.
[13] Cronin JN, Borges JB, Crockett DC, Farmery AD, Hedenstierna G, Larsson A, et al. Dynamic single-slice CT estimates whole-lung dual-energy CT variables in pigs with and without experimental lung injury. Intensive Care Med Exp 2019;7 (1):59.
[14] Matute-Bello G, Frevert CW, Martin TR. Animal models of acute lung injury. Am J Physiol Lung Cell Mol Physiol 2008;295(3):L379–99.
[15] Yehya N. Lessons learned in acute respiratory distress syndrome from the animal laboratory. Ann Transl Med 2019;7(19):503.
[16] Kayesh MEH, Sanada T, Kohara M, Tsukiyama-Kohara K. Tree shrew as an emerging small animal model for human viral infection: a recent overview. Viruses 2021;13(8).
[17] Yao YG. Creating animal models, why not use the Chinese tree shrew (Tupaia belangeri chinensis)? Zool Res 2017;38(3):118–26.
[18] Chen G, Wang W, Meng S, Zhang L, Wang W, Jiang Z, et al. CXC chemokine CXCL12 and its receptor CXCR4 in tree shrews (Tupaia belangeri): structure, expression and function. PLoS One 2014;9(5):e98231.
[19] Zhang J, Xiao H, Bi Y, Long Q, Gong Y, Dai J, et al. Characteristics of the tree shrew humoral immune system. Mol Immunol 2020;127:175–85.
[20] Sanada T, Yasui F, Honda T, Kayesh MEH, Takano JI, Shiogama Y, et al. Avian H5N1 influenza virus infection causes severe pneumonia in the Northern tree shrew (Tupaia belangeri). Virology 2019;529:101–10.
[21] Ye L, He M, Huang Y, Zhao G, Lei Y, Zhou Y, et al. Tree shrew as a new animal model for the study of lung cancer. Oncol Lett 2016;11(3):2091–5.
[22] Che P, Wang M, Larson-Casey JL, Hu RH, Cheng Y, El Hamdaoui M, et al. A novel tree shrew model of pulmonary fibrosis. Lab Invest 2021;101(1):116–24.
[23] Heron M. Deaths: leading causes for 2018. Natl Vital Stat Rep 2021;70 (4):1–115.
[24] de Souza Xavier Costa N, Ribeiro Junior G, Dos Santos Alemany AA, Belotti L, Zati DH, Frota Cavalcante M, et al. Early and late pulmonary effects of nebulized LPS in mice: an acute lung injury model. PLoS One 2017;12(9): e0185474.
[25] Bendib I, Beldi-Ferchiou A, Schlemmer F, Surenaud M, Maitre B, Plonquet A, et al. Alveolar compartmentalization of inflammatory and immune cell biomarkers in pneumonia-related ARDS. Crit Care 2021;25(1):23.
[26] Helm E, Talakoub O, Grasso F, Engelberts D, Alirezaie J, Kavanagh BP, et al. Use of dynamic CT in acute respiratory distress syndrome (ARDS) with comparison of positive and negative pressure ventilation. Eur Radiol 2009;19(1):50–7.
[27] Vecchi V, Langer T, Bellomi M, Rampinelli C, Chung KK, Cancio LC, et al. Low-dose CT for quantitative analysis in acute respiratory distress syndrome. Crit Care 2013;17(4):R183.
[28] Mecozzi L, Mambrini M, Ruscitti F, Ferrini E, Ciccimarra R, Ravanetti F, et al. In-vivo lung fibrosis staging in a bleomycin-mouse model: a new micro-CT guided densitometric approach. Sci Rep 2020;10(1):18735.
[29] Zhou S, Zhu T, Wang Y, Xia L. Imaging features and evolution on CT in 100 COVID-19 pneumonia patients in Wuhan, China. *Eur Radiol* 2020;30 (10):5446–54.
[30] Mrozek JD, Smith KM, Bing DR, Meyers PA, Simonton SC, Connett JE, et al. Exogenous surfactant and partial liquid ventilation: physiologic and pathologic effects. Am J Respir Crit Care Med 1997;156(4 Pt 1):1058–65.
[31] Zhang X, Chen J, Xue M, Tang Y, Xu J, Liu L, et al. Overexpressing p130/E2F4 in mesenchymal stem cells facilitates the repair of injured alveolar epithelial cells in LPS-induced ARDS mice. Stem Cell Res Ther 2019;10(1):74.
[32] Thompson BT, Moss M. A new definition for the acute respiratory distress syndrome. Semin Respir Crit Care Med 2013;34(4):441–7.
[33] Force ADT, Ranieri VM, Rubenfeld GD, Thompson BT, Ferguson ND, Caldwell E, et al. Acute respiratory distress syndrome: the Berlin Definition. JAMA 2012;307(23):2526–33.
[34] Grainge C, Jugg BJ, Smith AJ, Brown RF, Jenner J, Parkhouse DA, et al. Delayed low-dose supplemental oxygen improves survival following phosgene-induced acute lung injury. Inhal Toxicol 2010;22(7):552–60.
[35] Liang Q, Zhou Q, Li J, Chen Z, Zhang Z, Liu R, et al. Validation of novel hub genes and molecular mechanisms in acute lung injury using an integrative bioinformatics approach. Acta Biochim Biophys Sin (Shanghai) 2021;53 (3):342–53.
[36] Song S, Fu Z, Guan R, Zhao J, Yang P, Li Y, et al. Intracellular hydroxyproline imprinting following resolution of bleomycin-induced pulmonary fibrosis. Eur Respir J 2021.
[37] Campredon A, Battistella E, Martin C, Durieu I, Mely L, Marguet C, et al. Using chest CT scan and unsupervised machine learning for predicting and evaluating response to lumacaftor-ivacaftor in people with cystic fibrosis. Eur Respir J 2021.
[38] Quirino TC, Ortolan LDS, Sercundes MK, Marinho CRF, Turato WM, Epiphanio S. Lung aeration in experimental malaria-associated acute respiratory distress syndrome by SPECT/CT analysis. PLoS One 2020;15(5):e0233864.
[39] Schachner ER, Spieler B. Three-dimensional (3D) lung segmentation for diagnosis of COVID-19 and the communication of disease impact to the public. BMJ Case Rep 2020;13(8).
[40] Jones HA, Clark RJ, Rhodes CG, Schofield JB, Krausz T, Haslett C. In vivo measurement of neutrophil activity in experimental lung inflammation. Am J Respir Crit Care Med 1994;149(6):1635–9.
[41] Musch G, Venegas JG, Bellani G, Winkler T, Schroeder T, Petersen B, et al. Regional gas exchange and cellular metabolic activity in ventilator-induced lung injury. Anesthesiology 2007;106(4):723–35.
[42] Rodrigues RS, Bozza FA, Hanrahan CJ, Wang LM, Wu Q, Hoffman JM, et al. (18) F-fluoro-2-deoxyglucose PET informs neutrophil accumulation and activation in lipopolysaccharide-induced acute lung injury. Nucl Med Biol 2017;48:52–62.
[43] Park J, Kim S, Lim H, Liu A, Hu S, Lee J, et al. Therapeutic effects of human mesenchymal stem cell microvesicles in an ex vivo perfused human lung injured with severe E. coli pneumonia. Thorax 2019;74(1):43–50.
[44] Lv D, Xu Y, Cheng H, Ke Y, Zhang X, Ying K. A novel cell-based assay for dynamically detecting neutrophil extracellular traps-induced lung epithelial injuries. Exp Cell Res 2020;394(2):112101.
[45] Song S, Fu Z, Guan R, Zhao J, Yang P, Li Y, et al. Intracellular hydroxyproline imprinting following resolution of bleomycin-induced pulmonary fibrosis. Eur Respir J 2022;59(5).
[46] Jurisic V, Terzic T, Colic S, Jurisic M. The concentration of TNF-alpha correlate with number of inflammatory cells and degree of vascularization in radicular cysts. Oral Dis 2008;14(7):600–5.
[47] Peres e Serra A, Parra ER, Eher E, Capelozzi VL. Nonhomogeneous immunostaining of hyaline membranes in different manifestations of diffuse alveolar damage. Clinics (Sao Paulo) 2006;61(6):497–502.